Ocean Engineering 135 (2017) 39–51

Contents lists available at ScienceDirect

Ocean Engineering

journal homepage: www.elsevier.com/locate/oceaneng

2D numerical study of wave and current-induced oscillatory non-cohesive soil liquefaction around a partially buried pipeline in a trench

Lunliang Duan[a], Chencong Liao[b,*], Dongsheng Jeng[a,c], Linya Chen[a]

[a] School of Civil Engineering, Southwest Jiaotong University, Chengdu 610031, China
[b] Department of Civil Engineering, Shanghai Jiao Tong University, Shanghai 200240, China
[c] Griffith School of Engineering, Griffith University Gold Coast Campus, Queensland, QLD 4222, Australia

ARTICLE INFO

Keywords:
Wave-current interactions
Porous seabed
Liquefaction
Partially buried pipeline
Critical backfill thickness

ABSTRACT

This paper proposes a two-dimensional (2D) coupled model for wave and current-seabed-pipeline interactions to examine oscillatory non-cohesive soil liquefaction around a partially buried pipeline in a trench. Unlike previous studies, two new features are included in this model: (1) wave-current interactions around the pipeline; and (2) fully coupled processes for the wave and current-seabed-pipeline system. In this study, the Reynolds Averaged Navier-Stokes (RANS) equations are applied to simulate the flow field around the pipeline, and Biot's poro-elastic theory for porous media is imposed to govern the soil response due to the wave-current loading. After being validated using data available in the literature, the 2D model is used to investigate the effects of the current velocity, the soil properties, and the wave characteristics on oscillatory non-cohesive soil liquefaction. Using the model, a function for the critical backfill thickness and the wave steepness under various flow and soil conditions is proposed to facilitate engineering practice.

1. Introduction

Offshore pipelines are engineering facilities that are used to transport oil and gas from offshore oilfields to land. The protection of pipelines has attracted attention from offshore engineers due to their complex interactions with the ocean environment. Because waves and currents are usually the predominant loadings for offshore pipelines, the hydrodynamic pressure that acts on the seabed will further affect the pore pressures and reduce the effective stresses within the seabed when waves and currents propagate over the water surface. With the increase of the pore pressure and the decrease of the effective stresses, some of the soil around the pipeline may become unstable or even liquefy. Once liquefaction occurs, the seabed will behave like a heavy fluid without any resistance to shear loads, and the resulting loss of shear resistance may cause further damage to the pipeline. Therefore, evaluations of the soil response under combined wave-current loading are essential for the safety of pipelines.

Over the past few decades, numerous studies have been devoted to the mechanisms of wave-seabed interactions (Hsu and Jeng, 1994; Mei and Foda, 1981; Okusa, 1985; Thomas, 1989; Yamamoto et al., 1978; Ye and Jeng, 2011a; Corvaro et al., 2014a, 2014b). In these studies, the wave-induced pore pressures, stresses and displacements within the saturated and unsaturated seabed are examined, and the soil permeability and shear modulus are assumed to be constant. As an extension of the well-known Biot's poro-elastic theory, Zienkiewicz et al. (1980) proposed the one-dimensional *u-p* approximation for wave propagation over a porous seabed, which considered the acceleration of the soil displacement. Later, the one-dimensional *u-p* approximation was extended to the two-dimensional *u-p* approximation to examine the effective stresses in a porous seabed of finite thickness (Jeng and Rahman, 2000). Ulker et al. (2009) summarized the various formulations of the governing equations and their applications for wave-induced seabed responses. The interactions between waves and currents is another important phenomenon in the ocean environment. The existence of a current may remarkably alter the behavior of ocean waves (Kemp and Simons, 1983). Recently, wave-current interactions have been considered in studies of the seabed response (Liao et al., 2013; Ye and Jeng, 2011b; Zhang et al., 2013). However, these investigations only discussed the mechanisms of wave and current-seabed interactions for cases in which a pipeline was not involved. As a basic approximation of the soil response, these studies laid a foundation to further explore wave and current-seabed-pipeline interactions.

When a pipeline is considered in the interactions of a fluid-seabed-pipeline system, the problem becomes more complicated in the case of turbulent flow around the pipeline (Mattioli et al., 2012, 2013). Nevertheless, several investigations of wave and current-seabed-pipe-

* Corresponding author.
E-mail address: billaday@sjtu.edu.cn (C. Liao).

http://dx.doi.org/10.1016/j.oceaneng.2017.02.036
Received 4 April 2016; Received in revised form 16 December 2016; Accepted 27 February 2017
0029-8018/ © 2017 Elsevier Ltd. All rights reserved.

line interactions have been performed since the 1970s (MacPherson, 1978; Cheng and Liu, 1986; McDougal et al., 1988), which studied the wave-induced forces that act on a buried pipeline. Jeng (2001) examined the internal stresses within a pipeline using a finite element model. This model was extended to investigate the interactions between nonlinear waves, a buried pipeline and a porous seabed (Gao et al., 2003). Later, the influences of contact effects and inertial effects on the wave-induced seabed response around a pipeline were examined using a finite element model (Luan et al., 2008). Recently, Zhang et al. (2011) proposed a three-dimensional model to analyze the wave-induced seabed dynamic response around a pipeline. The effects of cross-anisotropic soil behavior on the wave-induced seabed response were also examined using a 2D numerical model (Zhao et al., 2016). It should be noted that these studies only considered wave loading and ignored the effects of the current, even though waves and currents usually coexist in the ocean environment. In addition, those investigations focused on fully buried pipelines, while partially buried pipelines are typically used in engineering practice to reduce costs and accelerate the construction process. Zhao et al. (2014) explored the effects of the backfill thickness on the soil response around a partially buried pipeline; however, only wave loading was considered. In addition, Zhao's model mainly considered the wave-induced residual soil response, while this study focuses on the oscillatory mechanism under combined wave-current loading.

This study proposes a coupled model for wave and current-seabed-pipeline interactions to examine the oscillatory non-cohesive soil response around a partially buried pipeline. RANS equations are combined with the k-ε turbulence model for the wave and current simulations, and Biot's poro-elastic theory is imposed to govern the soil response. The model is validated with data from previous studies in Section 3. A series of analyses of the oscillatory non-cohesive soil liquefaction potential is conducted in Section 4. Based on the numerical results, the critical thickness of the backfill material for protection against liquefaction can be estimated using the regression method.

2. Theoretical formulations

The numerical model includes two sub-models: a wave-current model and a seabed model with a partially buried pipeline. The wave-current model is used to describe the flow field, and the seabed model is used to determine the oscillatory non-cohesive soil response around a partially buried pipeline under combined wave-current loading.

Fig. 1 shows a sketch of the model of wave and current-seabed-pipeline interactions, where x and z are the Cartesian coordinates, h is the seabed depth, W is the width of the trench, B is the height of the trench, d is the water depth, H_b is the thickness of the backfill material, U_O is the initial current velocity, e is the distance from the seabed surface to the top of the backfill, C is a point below the pipeline, and L_s is the length of the computational domain in the transverse direction. In this study, L_s is set to three times the wavelength based on pre-test results to ensure that the influences of the boundary conditions on the flow field around the pipeline can be ignored.

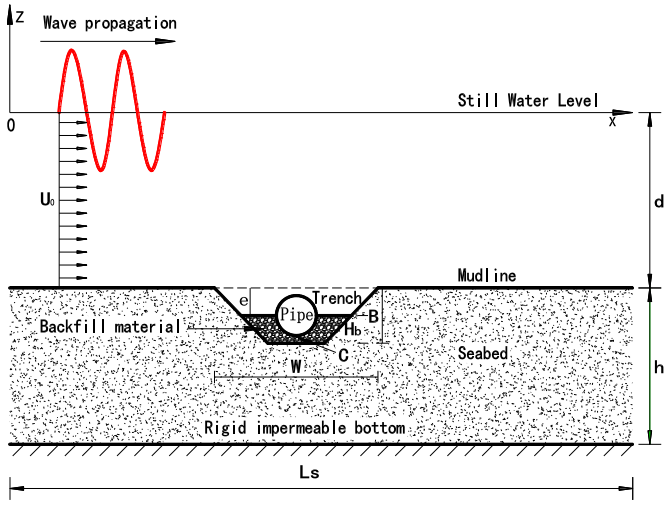

Fig. 1. Sketch of the model for wave and current-seabed-pipeline interactions.

2.1. Wave-current model

In the wave-current sub-model, the wave is generated by adding the momentum source functions to the source terms of the momentum conservation equation. The current is then simulated by imposing a steady inlet velocity on the upstream boundary and a pressure outlet on the downstream boundary, on which the pressure should be zero to ensure that the water can flow freely from the outlet. In addition, the wave-current model is constructed with a genuine free surface system, and the Level Set Method (LSM) is used to track the interface between the water and the air.

The RANS equations with a standard turbulence model are applied to simulate the flow field. For a 2D problem, the mass conservation equation and the momentum conservation equation can be written as follows

$$\frac{\partial \langle u_i \rangle}{\partial x_i} = 0 \tag{1}$$

$$\frac{\partial \langle u_i \rangle}{\partial t} + \frac{\partial \langle u_i \rangle \langle u_j \rangle}{\partial x_j} = -\frac{1}{\rho}\frac{\partial \langle p \rangle}{\partial x_i} + \frac{1}{\rho}\frac{\partial \tau_{ij}}{\partial x_j} + g_i + S_i \tag{2}$$

where x_i is the Cartesian coordinate, $()_i$ and $()_{ij}$ represent the index tensor notion, t is the time, $\langle u_i \rangle$ and $\langle p_i \rangle$ denote the ensemble averaged velocity and pressure of the fluid field, respectively, ρ is the fluid density, g_i is the acceleration of gravity, and S_i=(S_x, S_y, S_z) is an arbitrary source term. For the internal wave-maker method that is used in this study, the momentum source functions are applied to the source terms S_x, S_y and S_z of the RANS equations. The expressions for S_x, S_y, and S_z can be given as follows

$$S_x = -g(2\beta x)\exp(-\beta x^2)\frac{D_s}{w}\sin(kz - wt) \tag{3}$$

$$S_y = 0 \tag{4}$$

$$S_z = g\exp(-\beta x^2)\frac{kD_s}{w}\cos(kz - wt) \tag{5}$$

where w denotes the wave's angular frequency, k denotes the wave number, β=80/δ^2/L^2, in which L is the wavelength and δ is a parameter for the width of the internal generation region, and D_s is a parameter that can be expressed as

$$D_s = \frac{2A(w^2 - \alpha_1 g k^4 d^3)\cos\theta}{wI_1 k[1 - \alpha(kd)^2]} \tag{6}$$

where A is the wave amplitude, θ is the wave direction, $I_1 = \sqrt{\pi/\beta}\exp(-k^2/4\beta)$, α_1=α+1/3, and α is another parameter, which can be expressed by

$$\alpha = \frac{z_\alpha}{d}\left(\frac{z_\alpha}{2d} + 1\right) \text{ where } z_\alpha = -0.53d \tag{7}$$

Additional details can be found in Choi and Yoon (2009). The stress tensor, which includes the viscous stress and the Reynolds stress, is represented by τ_{ij} and can be expressed as

$$\tau_{ij} = \upsilon\left[\frac{\partial \langle u_i \rangle}{\partial x_j} + \frac{\partial \langle u_j \rangle}{\partial x_i}\right] - \rho\langle u'_i u'_j \rangle \tag{8}$$

where ν is the dynamic viscosity, and $-\rho\langle u'_i u'_j \rangle$ is the Reynolds stress term, which is modeled by the k-ε turbulent model (Launder and

Spalding, 1974; Rodi, 1993). By applying the eddy stress assumptions, the Reynolds stress term can be estimated by

$$-\rho\langle u'_i u'_j\rangle = \mu_t\left(\frac{\partial u_i}{\partial x_j}+\frac{\partial u_j}{\partial x_i}\right)-\frac{2}{3}\rho\delta_{ij}k \tag{9}$$

in which μ_t is the turbulence viscosity, κ is the turbulence kinetic energy (TKE), and δ_{ij} is the Kronecker delta. Based on Eqs. (8) and (9), Eq. (2) can be written as

$$\frac{\partial\rho\langle u_i\rangle}{\partial t}+\frac{\partial\rho\langle u_i\rangle\langle u_j\rangle}{\partial x_j}=-\frac{\partial}{\partial x_i}\left[\langle p\rangle+\frac{2}{3}\rho k\right]+\frac{\partial}{\partial x_j}\left[\mu_{eff}\left(\frac{\partial\langle u_i\rangle}{\partial x_j}+\frac{\partial\langle u_j\rangle}{\partial x_i}\right)\right]+\rho g_i \tag{10}$$

where $\mu_{eff}=\mu+\mu_t$ is the total effective viscosity.

The standard or most commonly used equations for the κ-ε turbulence model can be expressed as (Launder and Spalding, 1974)

$$\frac{\partial\rho\kappa}{\partial t}+\frac{\partial\rho\langle u_j\rangle\kappa}{\partial x_j}=\frac{\partial}{\partial x_j}\left[\left(\mu+\frac{\mu_t}{\sigma_\kappa}\right)\frac{\partial\kappa}{\partial x_j}\right]+\rho P_\kappa-\rho\varepsilon \tag{11}$$

$$\frac{\partial\rho\varepsilon}{\partial t}+\frac{\partial\rho\langle u_j\rangle\varepsilon}{\partial x_j}=\frac{\partial}{\partial x_j}\left[\left(\mu+\frac{\mu_t}{\sigma_\varepsilon}\right)\frac{\partial\varepsilon}{\partial x_j}\right]+\frac{\varepsilon}{\kappa}(C_{\varepsilon 1}\rho P_\kappa-C_{\varepsilon 2}\rho\varepsilon) \tag{12}$$

$$\mu_t=\rho C_\mu\frac{\kappa^2}{\varepsilon} \tag{13}$$

where κ is the TKE, and ε is the dissipation rate of the TKE. The constant values in this model are calibrated by comprehensive data fitting for a wide range of turbulent flows (Rodi, 1993): C_μ=0.09, σ_κ=1.00, σ_ε=1.30, $C_{\varepsilon 1}$=1.44, and $C_{\varepsilon 2}$=1.92.

The LSM is used to track the interface between the water and air and can be expressed as

$$\frac{\partial\phi}{\partial t}+\nabla\cdot(u_i\phi)=\gamma\nabla\cdot\left(\varepsilon_{ls}\nabla\phi-\phi(1-\phi)\frac{\nabla\phi}{|\nabla\phi|}\right) \tag{14}$$

where ϕ is the level set function, ε_{ls} is the parameter that controls the interface thickness, and γ is the reinitialization parameter. Additional detailed information can be found in Olsson et al. (2007).

2.2. Seabed model

In the seabed sub-model, the porous seabed is considered to be elastic, unsaturated, and hydraulically permeable. Moreover, the soil skeleton and the pore fluid are assumed to be compressible and to obey Hooke's law. Biot's poro-elastic theory (Biot, 1941) is used to govern the soil response, which can be expressed as

$$\nabla^2 p_s-\frac{\gamma_w n_s\beta}{k_s}\frac{\partial p_s}{\partial t}=\frac{\gamma_w}{k_s}\frac{\partial}{\partial t}\left(\frac{\partial u_s}{\partial x}+\frac{\partial w_s}{\partial z}\right) \tag{15}$$

where $\nabla^2=\left(\frac{\partial^2}{\partial x^2},\frac{\partial^2}{\partial z^2}\right)$ is the Laplace's operator, p_s is the wave and current-induced pore pressure, γ_w is the unit weight of water, n_s is the soil porosity, k_s is the soil permeability, u_s and w_s are the soil displacements in the x- and z- directions, respectively, and β is the compressibility of the pore fluid, which can be expressed as

$$\beta=\frac{1}{K_w}+\frac{1-S_r}{P_{w0}} \tag{16}$$

where K_w is the true modulus of water (taken as 2×10^9 N/m^2), S_r is the degree of seabed saturation, and P_{w0} is the absolute water pressure.

Based on Terzaghi's principle, the relationships between the effective stresses and the pore pressure are given by

$$\frac{\partial\sigma'_{sx}}{\partial x}+\frac{\partial\tau_{sxz}}{\partial z}=\frac{\partial p_s}{\partial x} \tag{17}$$

$$\frac{\partial\tau_{sxz}}{\partial x}+\frac{\partial\sigma'_{sz}}{\partial z}=\frac{\partial p_s}{\partial z} \tag{18}$$

where τ_{sxz} is the shear stress, and σ'_{sx} and σ'_{sz} are the effective stresses in the x- and z- directions, respectively.

Based on linear elasticity theory, the relationships between the elastic effective stresses and the soil displacements are given by

$$\sigma'_{sx}=2G\left[\frac{\partial u_s}{\partial x}+\frac{\mu_s}{1-2\mu_s}\left(\frac{\partial u_s}{\partial x}+\frac{\partial w_s}{\partial z}\right)\right] \tag{19}$$

$$\sigma'_{sz}=2G\left[\frac{\partial w_s}{\partial z}+\frac{\mu_s}{1-2\mu_s}\left(\frac{\partial u_s}{\partial x}+\frac{\partial w_s}{\partial z}\right)\right] \tag{20}$$

$$\tau_{sxz}=G\left(\frac{\partial u_s}{\partial z}+\frac{\partial w_s}{\partial x}\right) \tag{21}$$

where the shear modulus (G) is related to Young's modulus (E) by Poisson's ratio μ_s in the form of G=E/2(1+μ_s).

By substituting Eqs. (19)–(21) into Eqs. (17) and (18), the equations of force equilibrium will finally become

$$G\nabla^2 u_s+\frac{G}{(1-2\mu_s)}\frac{\partial}{\partial x}\left(\frac{\partial u_s}{\partial x}+\frac{\partial w_s}{\partial z}\right)=\frac{\partial p_s}{\partial x} \tag{22}$$

and

$$G\nabla^2 w_s+\frac{G}{(1-2\mu_s)}\frac{\partial}{\partial z}\left(\frac{\partial u_s}{\partial x}+\frac{\partial w_s}{\partial z}\right)=\frac{\partial p_s}{\partial z} \tag{23}$$

in the x- and z- directions, respectively.

2.3. Boundary conditions

The oscillatory pore pressure and the displacements within the soil can be obtained by solving the governing Eqs. (15), (22) and (23) with approximate boundary conditions. Hence, several boundary conditions must be specified, including the wave-seabed boundary conditions, seabed-pipeline boundary conditions, boundary conditions at the bottom of the seabed, seabed-backfill material boundary conditions and boundary conditions at the free surface of the water.

2.3.1. Wave-seabed boundary conditions

It is commonly accepted that the vertical effective normal stresses and the shear stresses vanish at the surface of the seabed and that the pore pressure is equal to the wave pressure (Jeng, 2013)

$$/\sigma'_{sz}=0,\ \tau'_{sxz}=0 \text{ and } p_s=p_b \tag{24}$$

where p_b is the wave pressure at the seabed surface, which can be obtained from the wave-current model.

2.3.2. Seabed-pipeline boundary conditions

The pipeline is assumed to be impermeable and elastic, and the normal gradient of the pore pressure is zero along the pipeline's surface, which can be written as

$$\frac{\partial p_s}{\partial n}=0 \tag{25}$$

It is also assumed that there is no relative displacement between the seabed and the pipeline at the interface

$$u_s=u_{pipe},\ w_s=w_{pipe}. \tag{26}$$

2.3.3. Boundary conditions at the bottom of the seabed

For soil resting on an impermeable rigid base, zero displacement and no vertical flow occur at the bottom of the seabed, which can be expressed as

$$u_s = w_s = 0, \frac{\partial p_s}{\partial z} = 0. \quad (27)$$

2.3.4. Seabed-backfill material boundary conditions

In general, the soil displacements, normal effective stresses and pore pressure should be continuous at the interface between the seabed and the backfill material

$$p_s = p_{bs}, u_s = u_{bs}, w_s = w_{bs}, \sigma'_{sx} = \sigma_{x,bs}, \sigma'_{sz} = \sigma_{z,bs}, \tau'_{sxz} = \tau_{xz,bs}. \quad (28)$$

where the subscript "*bs*" denotes the soil response parameters in the backfill material.

2.3.5. Boundary conditions at the free surface of water

In the model, the actual pressure at the water surface should be equal to atmospheric pressure. Therefore, the relative pressure (p) at the water surface should be zero.

2.4. Integration of the flow and seabed models

The entire model is solved using the finite element method. The wave model is first constructed with the internal wave-maker method by imposing the momentum source functions on the source terms of the RANS equation, and a steady current velocity is then added on the upstream boundary to form a new flow model. The seabed model is modeled with the PDE interface in the finite element analysis procedure. Two types of mesh systems are adopted: a matching mesh system and a moving mesh system. The matching mesh system is used along the seafloor, and the mesh elements are much smaller than those in the seabed domain. The moving mesh system is used along the sea surface to track the interface between the air and water. Both the flow model and the seabed model are constructed in the same software environment, and the wave and current-induced oscillatory non-cohesive soil response around the partially buried pipeline can give feedback to the wave-current model to adjust the computation of the flow field in the same time step to ensure that the entire model is coupled.

2.5. Convergence of the FEM meshes

A case with a backfill thickness of 0.5 m is selected to examine the rationality of the mesh system. For this case, the finite element model with the mesh system consists of 150,670 elements (including the wave generation zone, the wave absorber zone and the computational zone). Fig. 2 illustrates the mesh system around the pipeline for this case, and Fig. 3 shows the wave and current-induced maximum excess pore pressures at point *C* (Fig. 1) for the different mesh systems (expressed

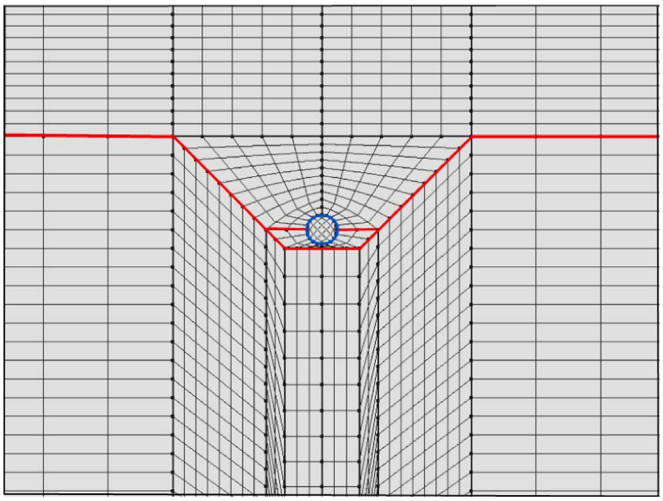

Fig. 2. Mesh system around the partially buried pipeline in this study.

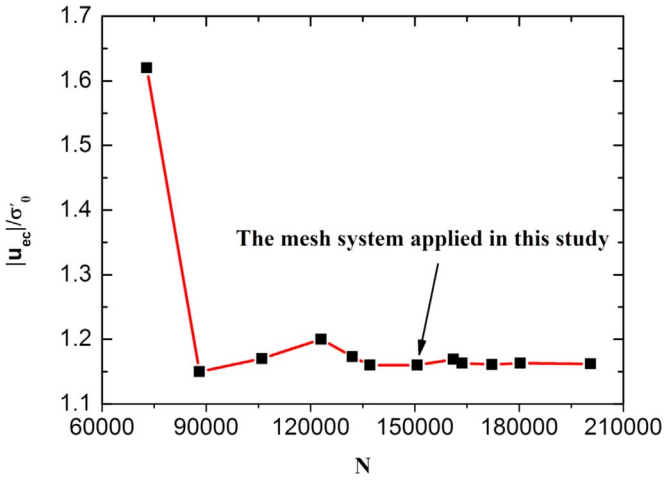

Fig. 3. Variations of the wave and current-induced maximum excess pore pressure ($|u_{ec}|/\sigma'_O$) at point *C* in Fig. 1 for various mesh systems.

Table 1
Parameters used in the first validation.

Parameters	Value	Unit
Wave period (T)	0.9	s
Water depth (d)	5	m
Seabed thickness (h)	1.8	m
Soil permeability (k_s)	1.8×10^{-4}	m/s
Shear modulus (G)	1.27×10^{7}	N/m^2
Poisson's ratio (μ_s)	0.3	–
Soil porosity (n_s)	0.425	–
Degree of saturation (S_r)	0.975	–

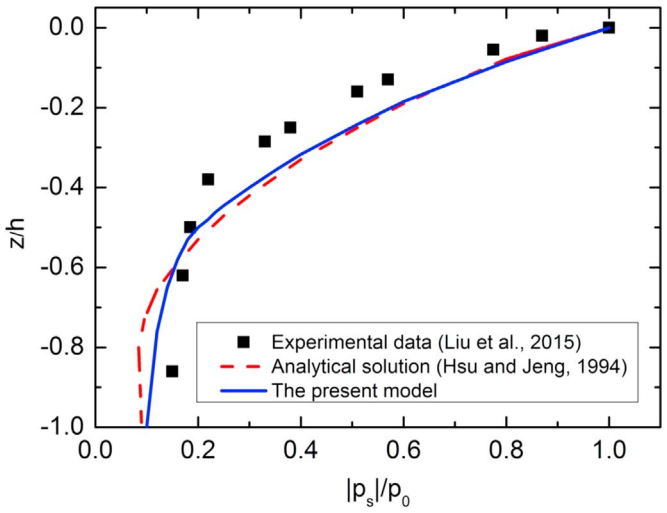

Fig. 4. Vertical distributions of the maximum pore pressure ($|p_s|/p_O$) versus seabed depth (z/h).

Table 2
Parameters used in the second validation.

Parameters	Value	Unit
Wave period (T)	2	s
Water depth (d)	0.3	m
Wave height (H)	0.1	m
Distance from the lower edge of the pipeline to the wall (e)	0	m
Pipeline diameter (D)	0.1	m
Keulegan-Carpenter number (KC)	13.67	–
Reynolds number (Re)	1.76×10^{4}	–
Ursell number (U_r)	38.93	–

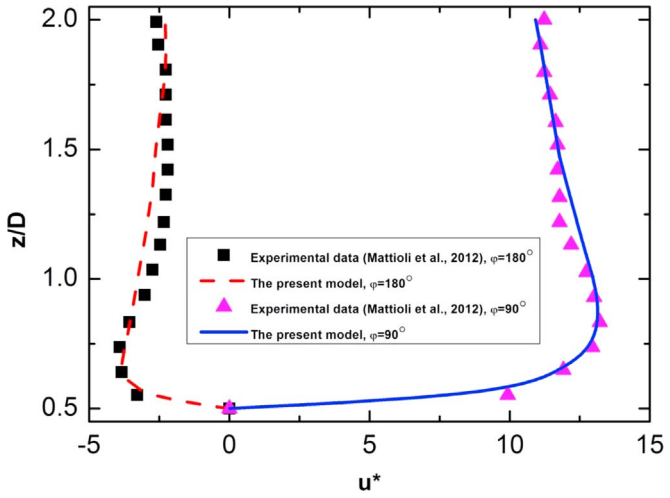

Fig. 5. Profiles of the dimensionless horizontal velocity component (u^*) along the vertical line through the center of the pipeline (z/D) for wave phases of φ=90° and φ=180°.

Table 3
Parameters used in the third validation.

Parameters	Value	Unit
Water depth (d)	0.533	m
Pipeline diameter (D)	0.168	m
Burial depth (e)	0.107	m
Trench width (L_{tr})	4.57	m
Trench depth (S)	0.826	m
Seabed porosity (n_s)	0.42	–
Young's modulus (E)	1.76×10^6	N/m^2
Poisson's ratio (μ_s)	0.33	N/m^2
Soil permeability (k_s)	1.1×10^{-3}	m/s

by the total number of elements N), in which $|u_{ec}|$ is the maximum excess pore pressure, and σ'_O is the initial effective stress at point C. As shown in Fig. 3, the mesh system achieves satisfactory computational accuracy.

3. Model validation

In this section, the 2D model will be validated by comparing it with previous data from the literature, including analytical solutions, numerical results and laboratory experimental data. However, because of the lack of investigations on the oscillatory soil response around partially buried pipelines in a trench, the model may be validated by reducing it to a simple case that involves interactions between waves, soil and a pipeline. The validations of the present model consist of three cases.

The first validation is to compare the model with the analytical solutions (Hsu and Jeng, 1994) and laboratory experimental data (Liu et al., 2015) for the case without a pipeline under wave loading. In this validation, the model should be simplified to the case of wave-seabed interactions to ensure that the sketch of the model is completely consistent with the model of Liu et al. (2015). The input data are listed in Table 1.

Fig. 4 shows the vertical distributions of the maximum wave-induced pore pressure (p_s/p_O) within the seabed with depth (z/h), in which $|p_s|$ denotes the maximum wave-induced pore pressure, and p_O denotes the amplitude of the dynamic wave pressure at the seabed surface. The results of the model agree well with the analytical solutions (Hsu and Jeng, 1994) and have the same trend as the experimental data (Liu et al., 2015).

The second validation compares the model with laboratory experimental data (Mattioli et al., 2012) for the case of a rigid bed, in which

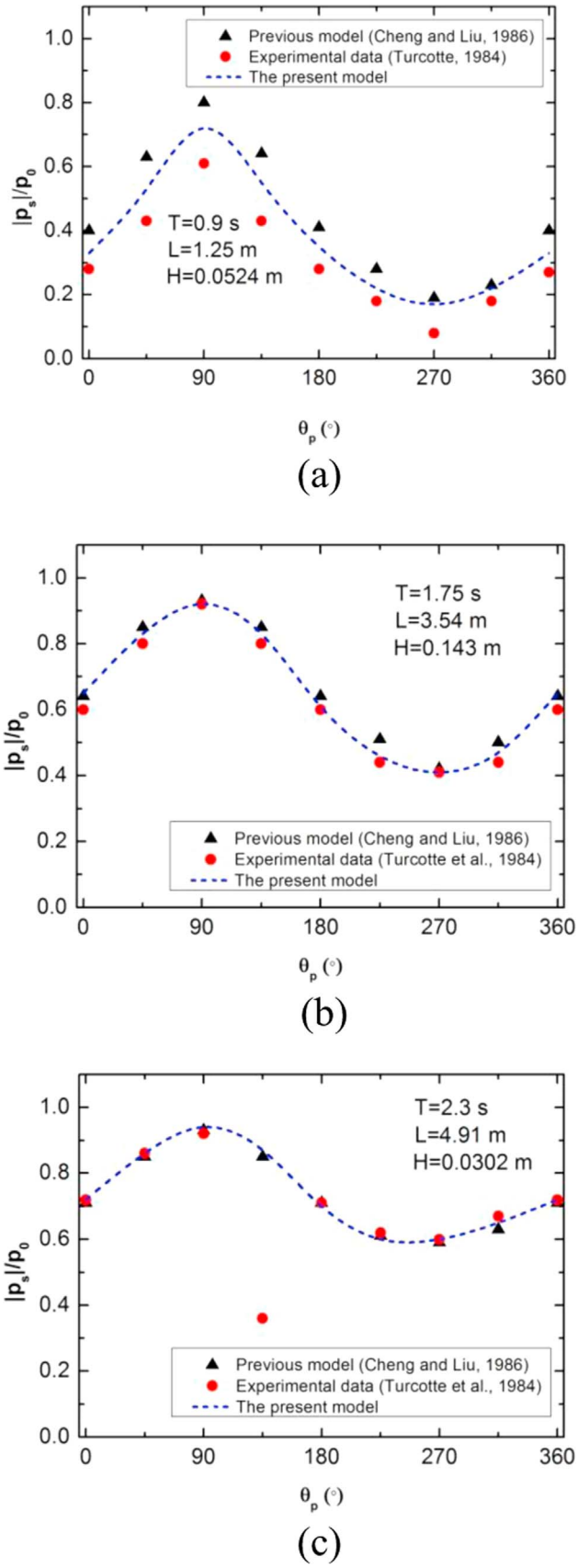

Fig. 6. Distributions of the maximum pore pressure ($|p_s|/p_O$) along the periphery of the pipeline (θ_p) for three wave conditions: (a) T=0.9 s, L=1.25 m, H=0.0524 m; (b) T=1.75 s, L=3.54 m, H=0.143 m; (c) T=2.3 s, L=4.91 m, H=0.0302 m.

Table 4
Input data for the numerical study.

Wave Parameters			
Wave height (H)	1.5 (m)	Wave period (T)	10 (s)
Water depth (d)	16 (m)		
Seabed Parameters			
Seabed thickness (h)	30 (m)	Seabed permeability (k_{sO})	1.0×10^{-7} (m/s)
Shear modulus (G)	1.0×10^{7} (N/m^2)	Degree of saturation (S_r)	0.98
Seabed porosity (n_s)	0.425	Poisson's ratio (μ_s)	0.35
Pipeline Parameters			
Young's modulus (E_p)	2.09×10^{11} (N/m^2)	Pipeline diameter (D)	0.8 (m)
Burial depth (e)	2.5 (m)	Poisson's ratio (μ_p)	0.32
Backfill Parameters			
Shear modulus (G_s)	1.0×10^{7} (N/m^2)	Soil permeability (k_s)	1.0×10^{-6} (m/s)
Trench width (W)	8 (m)	Trench height (B)	3 (m)
Backfill thickness (H_b)	0.5 (m)		
Current parameter			
Current velocity (U_O)	+1 (m/s)		

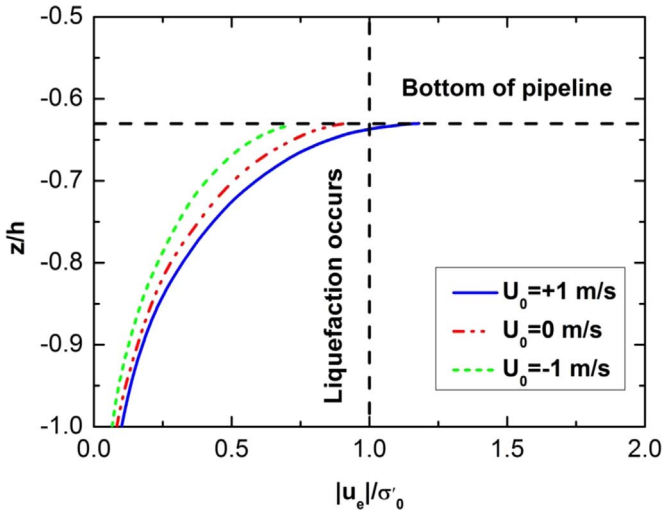

Fig. 8. Distributions of the maximum excess pore pressure ($|u_e|/\sigma'_0$) near the wave troughs along the vertical line through the center of the pipeline (z/h) for current velocities of U_0=−1 m/s, 0 m/s, and +1 m/s. These results are for the case in which H=1.5 m, T=10 s, d=16 m, k_s=1.0×10^{-6} m/s, S_r=0.98, H_b=0.5 m, U_O=0 represents only a wave with no current, $U_O > 0$ means that the wave travels in the direction of the current, and $U_O < 0$ means that the wave travels against the current.

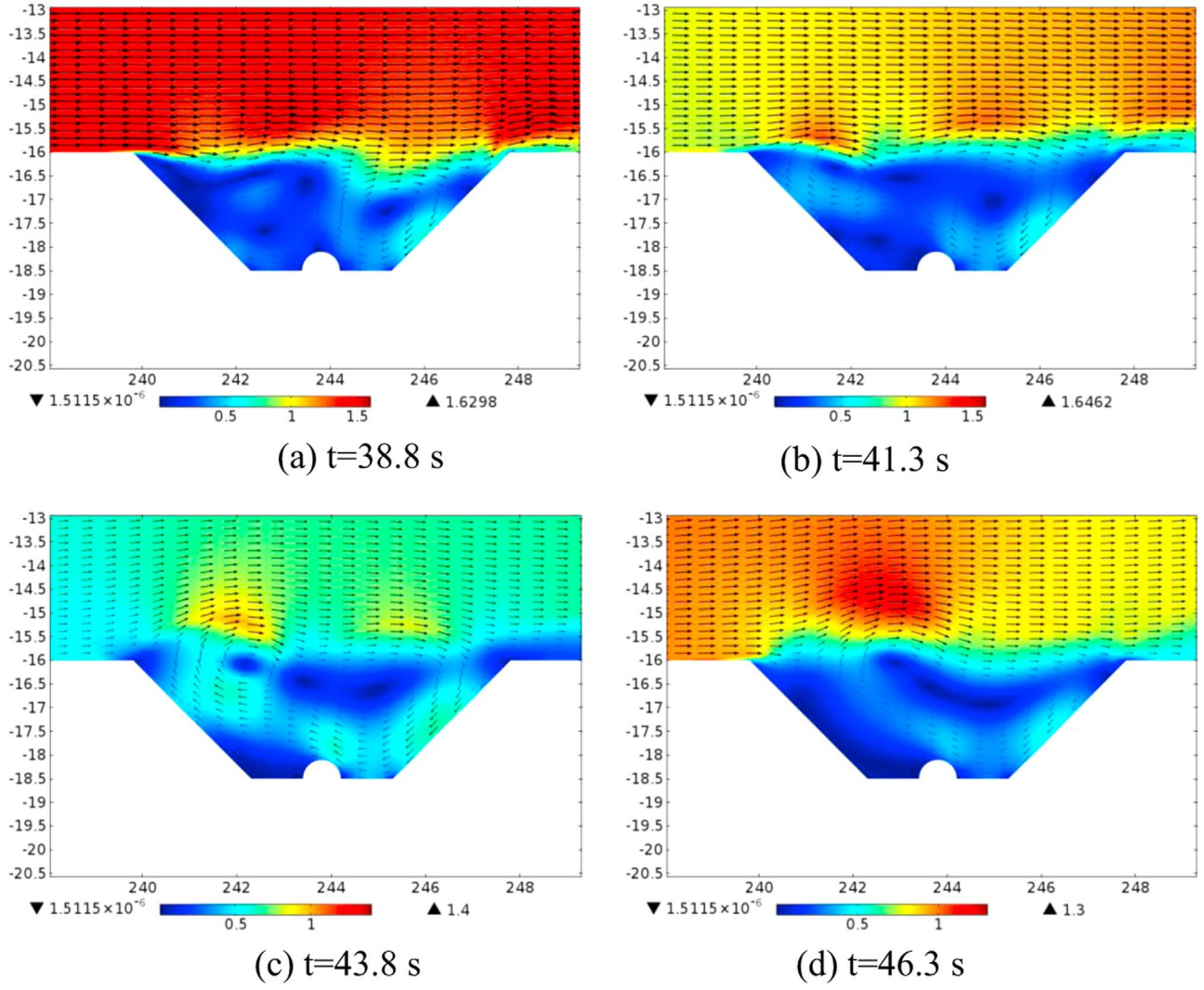

Fig. 7. Variations of the flow field around the partially buried pipeline with time.

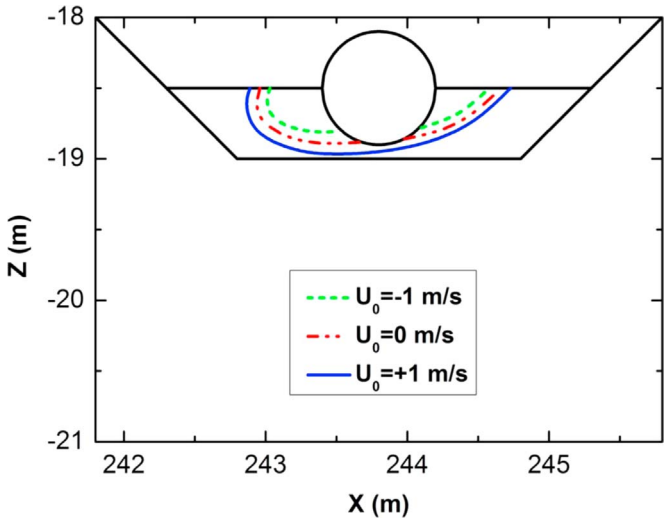

Fig. 9. Distributions of the liquefaction depth around the partially buried pipeline for current velocities of U_0=−1 m/s, 0 m/s, and +1 m/s. These results are for the case in which H=1.5 m, T=10 s, d=16 m, k_s=1.0×10^{-6} m/s, S_r=0.98, H_b=0.5 m, U_O=0 represents only a wave with no current, $U_O > 0$ means that the wave travels in the direction of the current, and $U_O < 0$ means that the wave travels against the current.

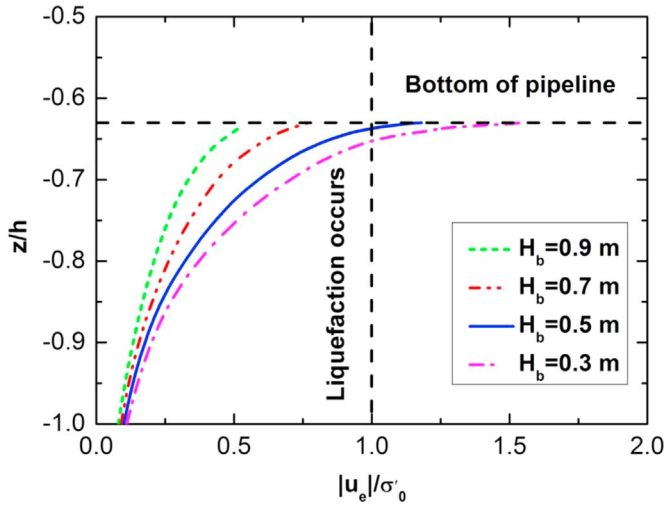

Fig. 10. Distributions of the maximum excess pore pressure ($|u_e|/\sigma'_0$) near the wave troughs along the vertical line through the center of the pipeline (z/h) for backfill thicknesses of H_b=0.3 m, 0.5 m, 0.7 m, and 0.9 m. These results are for the case in which U_0=+1 m/s, H=1.5 m, T=10 s, d=16 m, k_s=1.0×10^{-6} m/s, S_r=0.98, and both the wave and the current propagate in the direction of the positive x axis.

the center of the pipeline is located at the coordinate origin. In this validation, the model should be simplified to the case of wave-pipeline interactions to ensure that the sketch of the model is completely consistent with that of Mattioli et al. (2012). The input data are listed in Table 2.

Fig. 5 shows profiles of the dimensionless horizontal velocity component (u^*) along the vertical line through the center of the pipeline (z/D), in which the wave phase (φ) varies from 90° to 180° with an increment of 90°, and $u^*=u/(H/T)$, where u denotes the horizontal velocity. The results show that the dimensionless horizontal velocity profiles in the model generally agree with the experimental data (Mattioli et al., 2012).

The third validation is performed by comparing the model with laboratory experimental data (Turcotte et al., 1984) and numerical results (Cheng and Liu, 1986) for the case of a fully buried pipeline. Turcotte et al. (1984) conducted wave tank tests to study the wave-induced soil response around a fully buried pipeline. Later, Cheng and Liu (1986) examined the wave tank tests of Turcotte et al. (1984) with a numerical method. In the third validation, the model should be reduced to a simple case in which the interaction between the wave and seabed within a fully buried pipeline is consistent with the model of Cheng and Liu (1986). The parameters used in the comparison are shown in Table 3.

Fig. 6 compares the distributions of the maximum wave-induced pore pressure ($|p_s|/p_O$) along the periphery of the pipeline (θ_p) under three wave conditions: (a) T=0.9 s, L=1.25 m, H=0.0524 m; (b) T=1.75 s, L=3.54 m, H=0.143 m; and (c) T=2.3 s, L=4.91 m, H=0.0302 m. The results show that the model can capture the essential features of the numerical results (Cheng and Liu, 1986) and the laboratory experimental data (Turcotte et al., 1984).

The three comparisons demonstrate that the model can accurately predict the flow-seabed-pipeline interactions.

4. Results and discussion

The new contribution of this study is the inclusion of the wave-current interactions in the wave and current-seabed-pipeline system. Using the proposed model, the effects of the current, the soil properties, and the wave characteristics on the oscillatory non-cohesive soil liquefaction are investigated in detail. A criterion that includes the initial stress due to pre-consolidation is used to determine the oscillatory soil liquefaction (Zen and Yamazaki, 1990), which can be written as

$$\sigma'_0 + u_e \le 0 \tag{29}$$

where σ'_O is the initial effective stress, and $u_e=p_b-p_s$ denotes the excess pore pressure.

In this study, when examining the effects of a variable on the wave and current-induced oscillatory non-cohesive soil liquefaction around a partially buried pipeline, the values of other variables are kept fixed, and both the wave and the current propagate in the direction of the positive x axis. The following numerical examples use the parameters shown in Table 4 unless otherwise specified.

4.1. Initial consolidation and wave field

In the real ocean environment, the seabed has experienced consolidation due to its self-weight, and the initial consolidation can significantly affect the soil response around marine structures (Jeng, 2013). Therefore, it is essential to identify the initial effective stress (σ'_O) within the seabed when analyzing soil liquefaction. The model developed in this paper should be simplified to a case without a wave or current to determine the initial effective stress (σ'_O).

The trench and the pipeline are expected to affect the flow field near the trench. Consequently, a case with a backfill thickness of 0.5 m is selected to examine the effects of the partially buried pipeline in the trench on the flow field. Fig. 7 shows the distributions of the flow velocity field around the partially buried pipeline in a typical period. The flow velocity inside the trench is much lower than that outside the trench, and a vortex may occur in the trench due to flow separation at the trench edges because of the pressure gradient. In addition, the distributions of the flow velocity field around the partially buried pipeline is asymmetric. The left-right asymmetry of the flow field around the pipeline may be caused by the change in the flow regime in the trench due to the influences of the configurations of the trench and the pipeline.

4.2. Effects of currents

As reported in a previous study, a current can greatly affect the wave and current-induced soil response due to wave-current interactions (Zhang et al., 2013). Therefore, three current velocities (U_O=−1 m/s, 0 m/s, +1 m/s) are selected to examine the effects of a

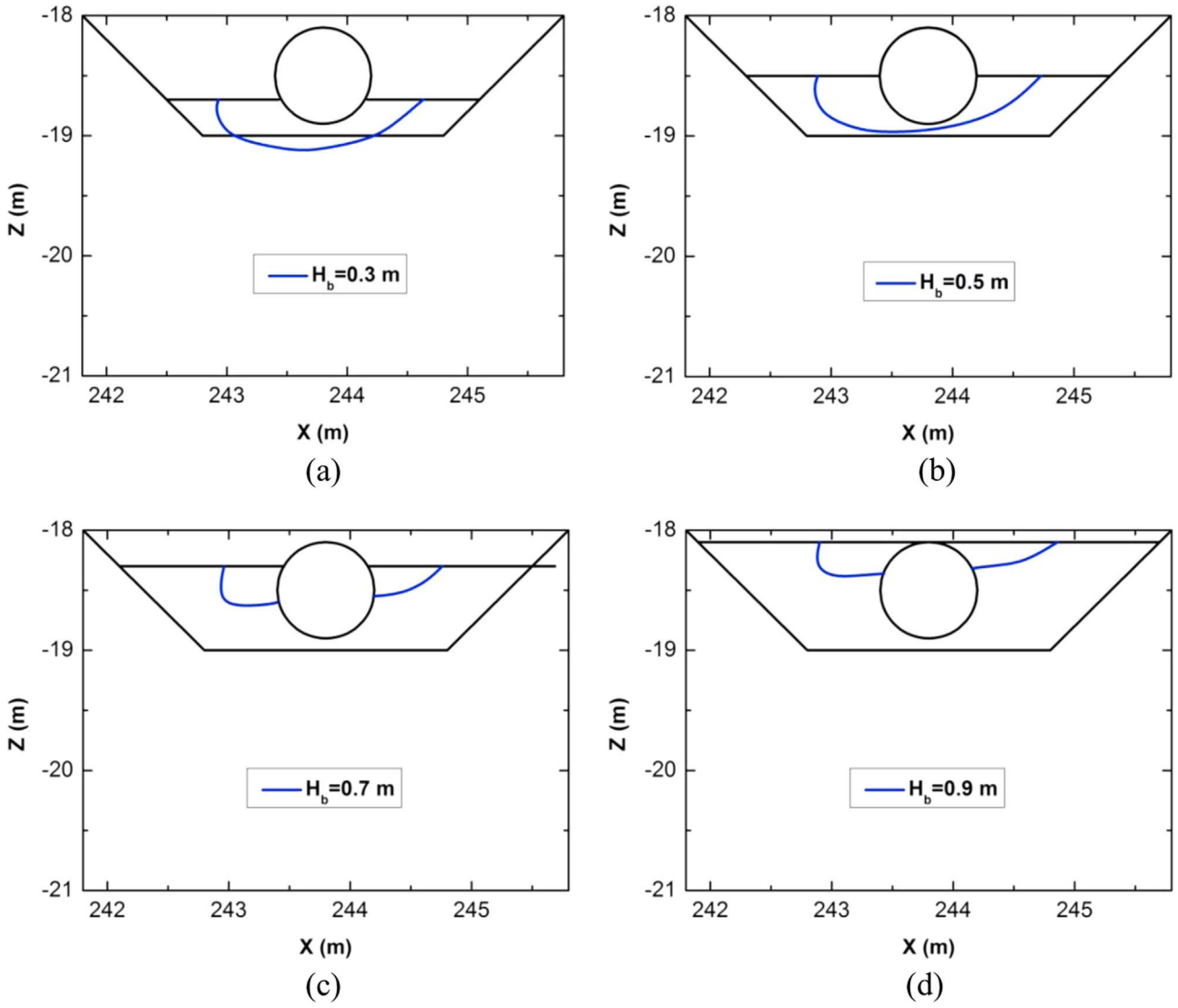

Fig. 11. Distributions of liquefaction depth around the partially buried pipeline for various backfill thicknesses: (a) H_b=0.3 m; (b) H_b=0.5 m; (c) H_b=0.7 m; (d) H_b=0.9 m. These results are for the case in which U_0=+1 m/s, H=1.5 m, T=10 s, d=16 m, k_s=1.0×10^{-6} m/s, S_r=0.98, and both the wave and the current propagate in the direction of the positive x axis.

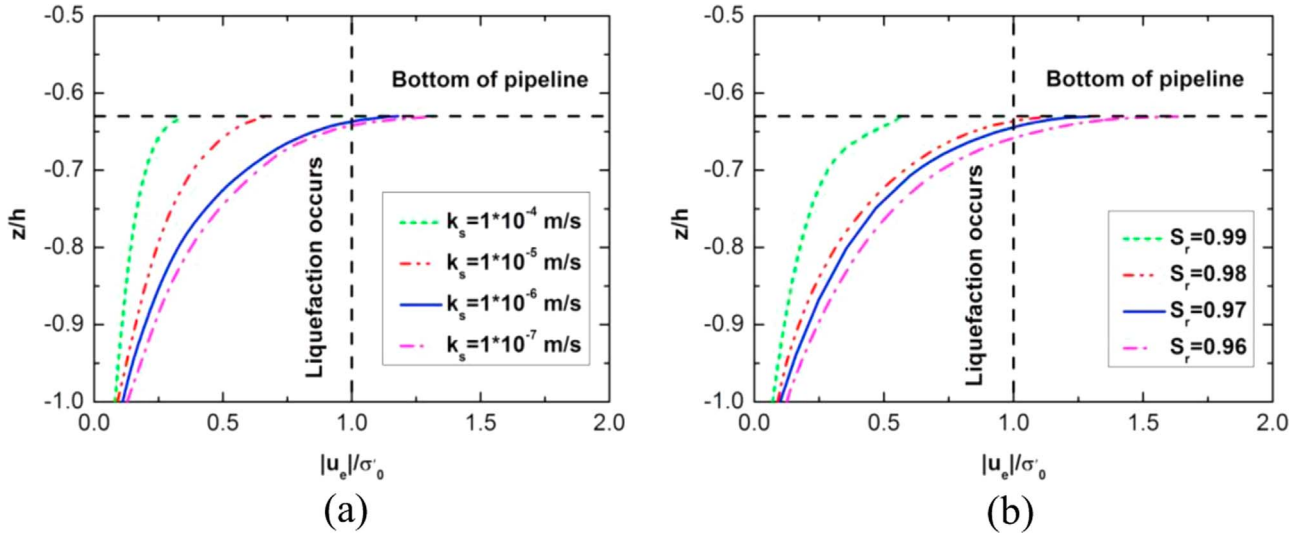

Fig. 12. Distributions of the maximum excess pore pressure ($|u_e|/\sigma'_o$) near the wave troughs along the vertical line through the center of the pipeline (z/h) for different soil properties: (a) k_s=1.0×10^{-4} m/s, 1.0×10^{-5} m/s, 1.0×10^{-6} m/s, 1.0×10^{-7} m/s, S_r=0.98; (b) k_s=1.0×10^{-6} m/s, S_r=0.96, 0.97, 0.98, 0.99. These results are for the case in which U_0=+1 m/s, H=1.5 m, T=10 s, d=16 m, H_b=0.5 m, and both the wave and the current propagate in the direction of the positive x axis.

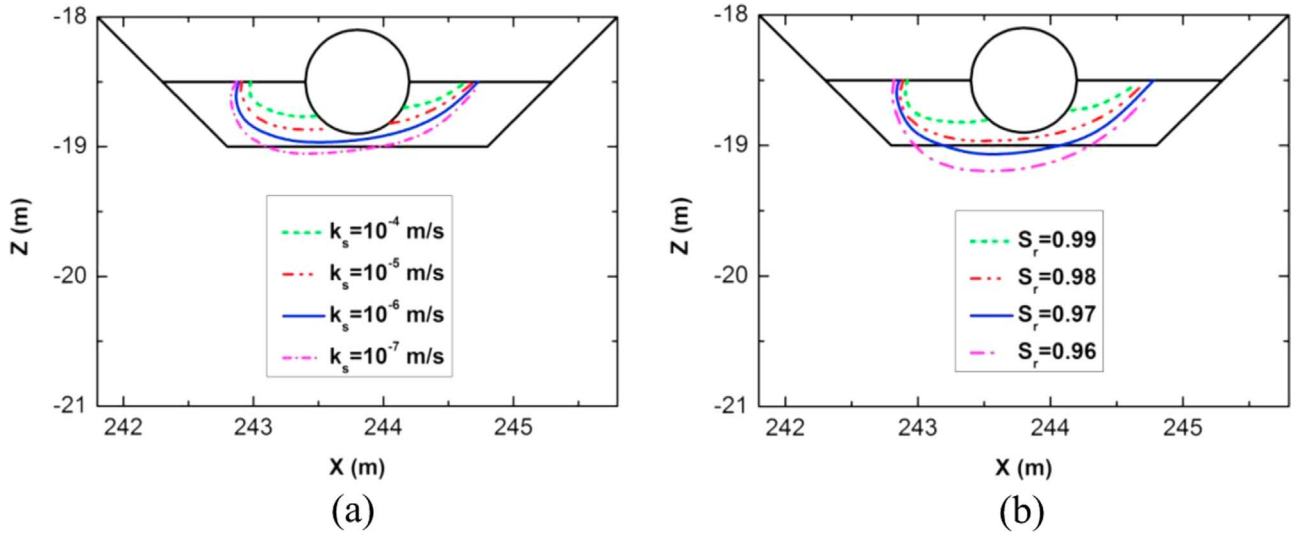

Fig. 13. Distributions of the liquefaction depth around the partially buried pipeline for different soil properties: (a) k_s=1.0×10^{-4} m/s, 1.0×10^{-5} m/s, 1.0×10^{-6} m/s, 1.0×10^{-7} m/s, S_r=0.98; (b) k_s=1.0×10^{-6} m/s, S_r=0.96, 0.97, 0.98, 0.99. These results are for the case in which U_0=+1 m/s, H=1.5 m, T=10 s, d=16 m, H_b=0.5 m, and both the wave and the current propagate in the direction of the positive x axis.

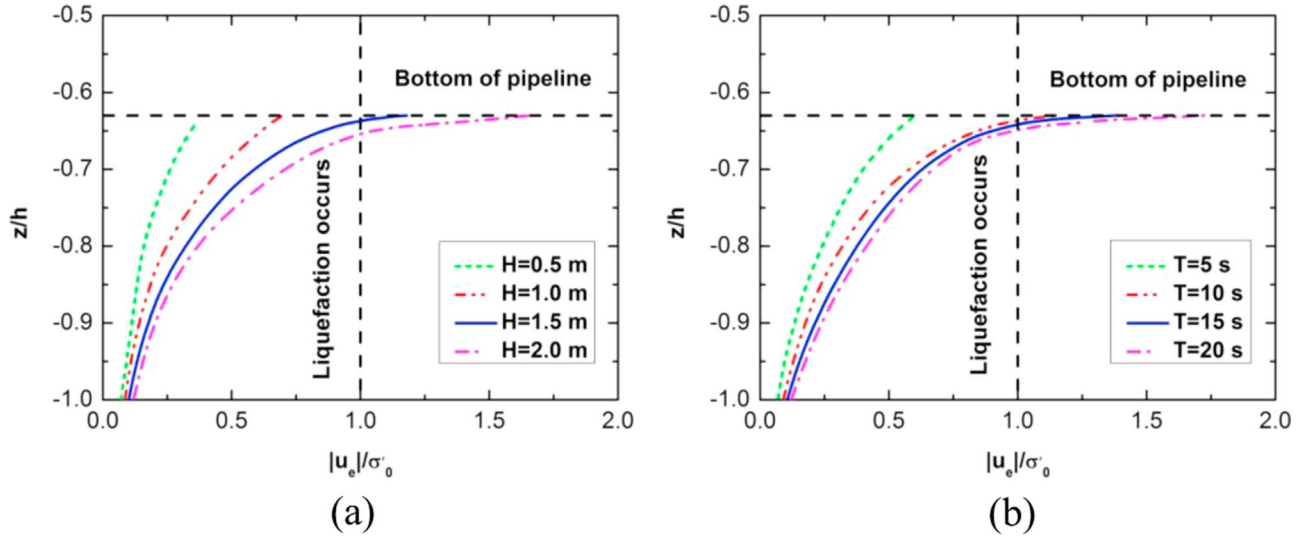

Fig. 14. Distributions of the maximum excess pore pressure ($|u_e|/\sigma'_O$) near the wave troughs along the vertical line through the center of the pipeline (z/h) for different wave conditions: (a) H=0.5 m, 1.0 m, 1.5 m, 2.0 m, T=10 s; (b) H=1.5 m, T=5 s, 10 s, 15 s, 20 s. These results are for the case in which U_0=+1 m/s, d=16 m, k_s=1.0×10^{-6} m/s, S_r=0.98, H_b=0.5 m, and both the wave and the current propagate in the direction of the positive x axis.

current on the wave and current-induced oscillatory non-cohesive soil liquefaction around the partially buried pipeline. The case with U_O=0 represents only a wave with no current, while $U_O > 0$ means that the wave travels in the direction of the current, and $U_O < 0$ means that the wave travels against the current. Fig. 8 shows the distributions of the maximum excess pore pressure ($|u_e|/\sigma'_O$) near the wave troughs along the vertical line through the center of the pipeline (z/h), in which $|u_e|$ is the amplitude of the excess pore pressure within the soil. Fig. 9 shows the distributions of the liquefaction depth around the pipeline under various current velocities. The results show that the maximum excess pore pressure ($|u_e|/\sigma'_O$) for the case of U_O=+1 m/s is greater than that for the case of U_O=−1 m/s (Fig. 8). In addition, the oscillatory liquefaction depth increases with increasing current velocity when the wave travels in the direction of the current (Fig. 9). This occurs because the wave that travels in the direction of the current can increase the wave pressure at the seabed surface (Ye and Jeng, 2011b), which will further affect the pore pressure within the soil. Moreover, the variations of the wave characteristics due to the wave-current interactions will change the phase difference between the wave pressure at the seabed surface and the pore pressure within the soil, and the numerical results in this study indicate that changes of the phase difference can increase the soil liquefaction potential. Fig. 9 also shows that the distributions of the liquefaction depth around the pipeline is left-right asymmetric, which may be due to the phase lags of the pore pressure within the soil under progressive wave loading.

4.3. Effects of soil properties

The soil properties are important factors that affect the wave and current-induced oscillatory non-cohesive response around a partially buried pipeline. In this section, the effects of the backfill thickness (H_b), the backfill permeability (k_s) and the degree of saturation (S_r) will be studied in detail.

To examine the effects of the backfill thickness (H_b) on the oscillatory soil response around the partially buried pipeline under combined wave-current loading, the backfill thickness is varied from

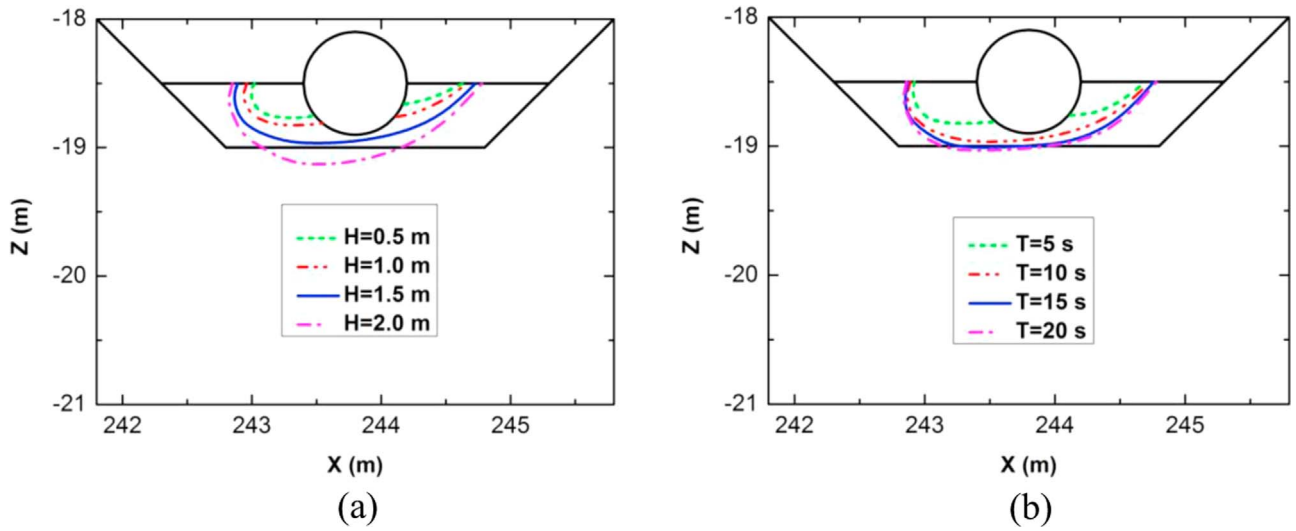

Fig. 15. Distributions of the liquefaction depth around the partially buried pipeline for different wave conditions: (a) H=0.5 m, 1.0 m, 1.5 m, 2.0 m, T=10 s; (b) H=1.5 m, T=5 s, 10 s, 15 s, 20 s. These results are for the case in which U_0=+1 m/s, d=16 m, k_s=1.0×10^{-6} m/s, S_r=0.98, H_b=0.5 m, and both the wave and the current propagate in the direction of the positive x axis.

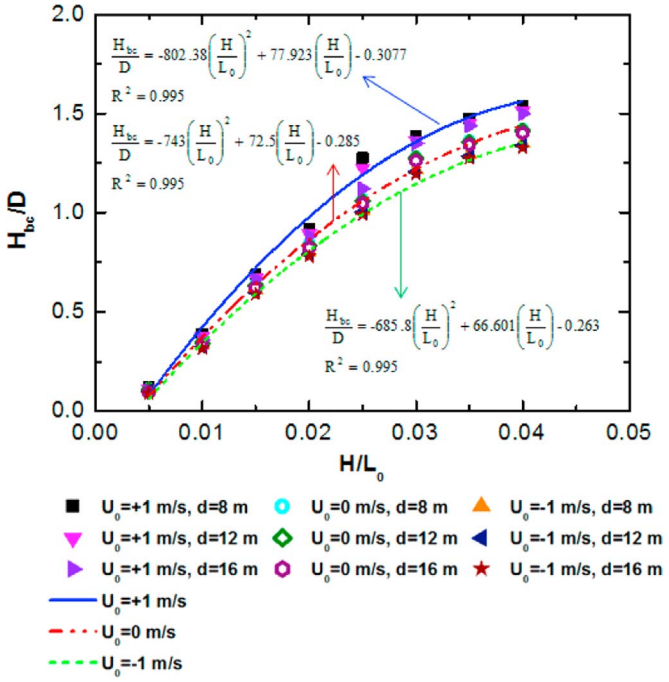

Fig. 16. Distributions of the critical backfill thickness (H_{bc}/D) versus wave steepness (H/L_O) for water depths of d=8 m, 12 m, and 16 m.

0.3m to 0.9 m at an interval of 0.2 m. Fig. 10 shows the distributions of the maximum excess pore pressure ($|u_e|/\sigma'_O$) near the wave troughs along a vertical line through the center of the pipeline (z/h) for the four backfill thicknesses, and Fig. 11 shows the distributions of the liquefaction depth around the partially buried pipeline for the same four backfill thicknesses (H_b). The distributions of the liquefaction depth is also left-right asymmetric due to the phase lags of the pore pressure under progressive wave loading. Moreover, Fig. 10 demonstrates that the maximum excess pore pressure decreases as the backfill thickness increases. Similarly, as shown in Fig. 11, the liquefaction depth at the bottom of the pipeline is greater for smaller backfill thicknesses. This occurs because both the flow field and the initial effective stress around the pipeline can be affected by the thickness of the backfill, and the variations of the flow field will further influence the wave pressures at the seabed surface and the pore pressures within the seabed. In other words, the maximum excess pore pressure is lower with a greater backfill thickness, in which the initial effective stress within the soil is higher. An additional conclusion is that the seabed under the pipeline becomes more difficult to liquefy with increasing backfill thickness. Thus, there should be a critical backfill thickness (H_{bc}) that can fully prevent the seabed at the bottom of the partially buried pipeline from being liquefied under certain conditions.

The backfill permeability (k_s) and the degree of seabed saturation (S_r) are also important for the wave and current-induced seabed response around a partially buried pipeline. Thus, four backfill permeabilities (k_s=1×10^{-4} m/s, 1×10^{-5} m/s, 1×10^{-6} m/s, 1×10^{-7} m/s) and four degrees of seabed saturation (S_r=0.96, 0.97, 0.98, 0.99) are selected for parametric studies.

Fig. 12 shows the distributions of the maximum excess pore pressure ($|u_e|/\sigma'_O$) near the wave troughs along the vertical line through the center of the pipeline (z/h), and Fig. 13 shows the distributions of the liquefaction depth under various soil conditions. The distributions of the liquefaction depth in Fig. 13 is similar to that in Fig. 9 due to the phase lags of the pore pressure under progressive wave loading. Furthermore, these results demonstrate that both the backfill permeability (k_s) and the degree of seabed saturation (S_r) can significantly affect the maximum excess pore pressure under the pipeline, and the seabed becomes easier be liquefy with decreasing backfill permeability (k_s) and degree of saturation (S_r). Therefore, coarse sand with high permeability can be used to reduce the liquefaction depth around a partially buried pipeline.

4.4. Effects of wave characteristics

In general, the wave characteristics play an important role in the seabed response. The wave height (H) can directly affect the wave forces on the seabed, and the wave period (T) can affect the pore pressure and effective stresses in the seabed by affecting the wavelength (L).

To explore the effects of the wave height (H) on the seabed response around the partially buried pipeline, the wave height (H) is varied from 0.5m to 2.0 m at an interval of 0.5 m. Figs. 14a and 15a show the distributions of the maximum excess pore pressure ($|u_e|/\sigma'_O$) along the vertical line through the center of the pipeline (z/h) and the liquefaction depths around the pipeline, respectively, for various wave heights. The results show that both the maximum excess pore pressure and the

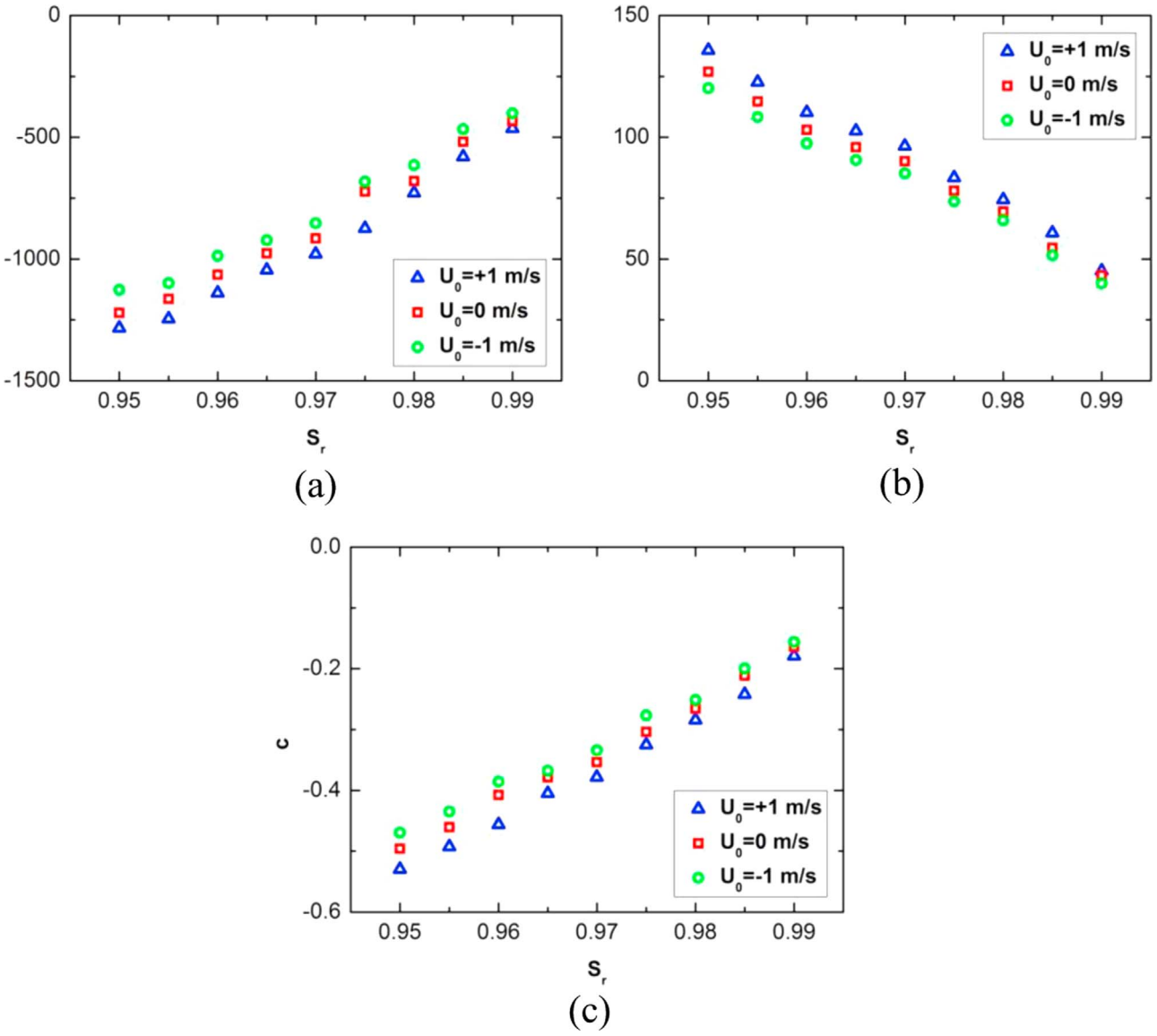

Fig. 17. Coefficients *a*, *b*, and *c* for different degrees of seabed saturation (S_r) from 0.95 to 0.99 at an increment of 0.005.

liquefaction depth under the partially buried pipeline increase as the wave height increases. In addition, the effects of the wave height on the liquefaction depth increase with increasing wave height. Four waves with different periods (T=5 s, 10 s, 15 s, 20 s) are generated to examine the effects of the wave period. Figs. 14b and 15b show the distributions of the maximum excess pore pressure ($|u_e|/\sigma'_O$) along the vertical line through the center of the pipeline (z/h) and the liquefaction depth around the pipeline, respectively, for various wave periods. The left-right asymmetry of the liquefaction depth around the pipeline in Fig. 15 is still similar to that in Fig. 9 due to the phase lags of the pore pressure in the soil under progressive wave loading. As shown in Fig. 14b, the wave and current-induced maximum excess pore pressure increases as the wave period increases. However, the effects of the wave period on the maximum excess pore pressure decrease with increasing wave period. Fig. 15b also demonstrates that the seabed at the bottom of the pipeline more easily liquefies with longer wave periods.

4.5. Application to engineering practice

To protect a pipeline against oscillatory soil liquefaction, a critical backfill thickness (H_{bc}) is required for engineering design. When the backfill thickness is less than H_{bc}, the bottom of the pipeline will be damaged by the wave and current-induced oscillatory soil liquefaction. On the other hand, the pipeline in the trench will be protected against the oscillatory soil liquefaction when the backfill thickness is greater than H_{bc}.

According to the preliminary study, the critical backfill thickness (H_{bc}) is related to the flow characteristics and the soil properties. Of these parameters, the wave height (H), the wave period (T), the backfill permeability (k_s) and the degree of seabed saturation (S_r) are all sensitive factors that control the distributions of the liquefaction depth under the partially buried pipeline; however, the numerical results indicate that the wave height (H) is the dominant factor. In this paper, the backfill material is assumed to be selected by the engineers to protect the pipeline; in other words, the engineers can select the backfill material described in Table 4. Therefore, the wave steepness (H/L_O) (where L_O is the linear wavelength without a current), the current velocity (U_O), and the degree of seabed saturation (S_r) are used to determine the critical backfill thickness (in terms of H_{bc}/D). The backfill permeability (k_s) is not included. To facilitate engineering practice, the method of estimating the critical backfill thickness should be as simple as possible while providing sufficient accuracy. Therefore,

Fig. 16 shows the relationship between the critical backfill thickness (H_{bc}/D) and the wave steepness (H/L_O) for various current velocities based on the numerical results of this study and the regression method used in Zhao and Jeng (2016), where the least squares algorithm is used to fit the curves. The results show that the water depth has a smaller effect than the other parameters and can be neglected. The relationship between the critical backfill thickness (H_{bc}/D) and the wave steepness (H/L_O) can be expressed as

$$\frac{H_{bc}}{D} = a\left(\frac{H}{L_0}\right)^2 + b\left(\frac{H}{L_0}\right) + c, \tag{30}$$

where $L_O=(gT^2/2\pi)\tan h(2\pi d/L_O)$ is the linear wavelength without a current.

The coefficients a, b, and c for various degrees of seabed saturation are plotted in Fig. 17, in which the critical backfill thickness is linked to the soil properties. The procedure for using Eq. (30), Figs. 16 and 17 to determine the critical backfill thickness for pipeline protection against seabed liquefaction for the particular trench geometry and soil conditions considered in this paper is as follows

(1) The wave steepness (H/L_O) can be determined from the wave characteristics;
(2) With the given current velocity and the soil properties (i.e., degree of seabed saturation), three coefficients (a, b, c) can be determined from Fig. 17;
(3) With the coefficients (a, b, c) obtained in Step (2), the relationship between H_{bc}/D and H/L_O can be obtained from Eq. (30);
(4) Using the wave steepness obtained in Step (1), the users can determine H_{bc}/D and then obtain the critical thickness of the backfill material (H_{bc}).

This procedure is based on the numerical examples that were presented in this paper. Additional investigations are required in the future to determine the effects of other parameters.

5. Conclusions

This study proposes a 2D coupled model for flow-seabed-pipeline interactions to investigate oscillatory non-cohesive soil liquefaction around a partially buried pipeline in a trench under combined wave-current loading. The effects of the current velocity, soil parameters and wave characteristics on the flow-induced non-cohesive soil response around the pipeline are examined. The following conclusions can be drawn from the numerical results:

(1) The validations show that the model can provide sufficiently accurate predictions of the flow-induced oscillatory pore pressure within the soil.
(2) The flow velocity inside the trench is much lower than that outside the trench, and a vortex may occur in the trench due to flow separation at the trench edges. In addition, the distributions of the flow field is left-right asymmetric along the vertical line through the center of the pipeline under progressive wave loading due to the influences of the trench and the pipeline.
(3) The liquefaction depth at the bottom of the pipeline decreases with increasing water depth (d), backfill thickness (H_b), backfill permeability (k_s) and degree of seabed saturation (S_r) but increases as the wave period (T) and the wave height (H) increase. However, the water depth (d) has a much smaller effect than the other parameters.
(4) The current velocity (U_O) can increase the liquefaction potential within the soil around a partially buried pipeline when the wave travels in the current direction, which should be considered when analyzing the oscillatory non-cohesive soil response due to wave-current interactions.
(5) The thickness of the backfill (H_b) plays an important role in the oscillatory soil liquefaction potential under wave-current loading, and the proposed function of the critical backfill thickness (H_{bc}/D) and the wave steepness (H/L_O) for a particular trench geometry under certain soil conditions could provide a reference for the protection of partially buried pipelines in engineering practice.

Acknowledgments

The authors are grateful for the financial support from the National Natural Science Foundation of China (Grant no. 41602282). The first author is grateful for the support of scholarship from the SWJTU Scholarship Council.

References

Biot, M.A., 1941. General theory of three-dimensional consolidation. J. Appl. Phys. 26, 155–164.
Cheng, A.H.D., Liu, P.L.F., 1986. Seepage force on a pipeline buried in a poroelastic seabed under wave loading. Appl. Ocean Res. 8, 22–32.
Choi, J., Yoon, S.B., 2009. Numerical simulations using momentum source wave-maker applied to RANS equation model. Coast. Eng. 56, 1043–1060.
Corvaro, S., Miozzi, M., Postacchini, M., Mancinelli, A., Brocchini, M., 2014a. Fluid-particle interaction and generation of coherent structures over permeable beds: an experimental analysis. Adv. Water Res. 72, 97–109.
Corvaro, S., Seta, E., Mancinelli, A., Brocchini, M., 2014b. Flow dynamics on a porous medium. Coast. Eng. 91, 280–298.
Gao, F.P., Jeng, D.S., Sekiguchi, H., 2003. Numerical study on the interaction between nonlinear wave, buried pipeline and non-homogeneous porous seabed. Comput. Geotec. 30, 535–547.
Hsu, J.R.C., Jeng, D.S., 1994. Wave-induced soil response in an unsaturated anisotropic seabed of finite thickness. Int. J. Numer. Anal. Met. 18, 785–807.
Jeng, D.S., 2001. Numerical modeling for wave-seabed-pipe interaction in a nonhomogeneous porous seabed. Soil Dyn. Earthq. Eng. 21, 699–712.
Jeng, D.S., 2013. Porous Models for Wave-seabed Interactions, first ed. London, New York.
Jeng, D.S., Rahman, M.S., 2000. Effective stresses in a porous seabed of finite thickness: inertia effects. Can. Geotech. J. 37, 1388–1397.
Kemp, P.H., Simons, R.R., 1983. The interaction of wave and a turbulent current: waves propagating against the current. J. Fluid Mech. 130, 73–89.
Launder, B.E., Spalding, D.B., 1974. The numerical computation of turbulence flows. Comput. Methods Appl. Mech. Eng. 3, 269–289.
Liao, C.C., Jeng, D.S., Zhang, L.L., 2013. An analytical approximation for dynamic soil response of a porous seabed due to combined wave and current loading. J. Coast. Res. 31, 1120–1128.
Liu, B., Jeng, D.S., Ye, G.L., 2015. Laboratory study for pore pressures in sandy deposit under wave loading. Ocean Eng. 106, 207–219.
Luan, M.T., Qu, P., Jeng, D.S., Guo, Y., Yang, Q., 2008. Dynamic response of a seabed-pipeline interaction under wave loading: soil-pipeline contact effects and inertial effects. Comput. Geotech. 35, 173–186.
MacPherson, H., 1978. Wave forces on pipeline buried in permeable seabed. J. Waterw. Port Coast. Ocean Div. ASCE 104, 407–419.
Mattioli, M., Alsina, J.M., Mancinelli, A., Miozzi, M., Brocchini, M., 2012. Experimental investigation of the nearbed dynamics around a submarine pipeline laying on different types of seabed: the interaction between turbulent structures and particles. Adv. Water Resour. 48, 31–46.
Mattioli, M., Mancinelli, A., Brocchini, M., 2013. Experimental investigation of the wave-induced flow around a surface-touching cylinder. J. Fluid. Struct. 37, 62–87.
McDougal, W.G., Davidson, S.H., Monkmeyer, P.L., Sollitt, C.K., 1988. Wave-induced forces on buried pipeline. J. Waterw. Port C.-ASCE 114, 220–236.
Mei, C.C., Foda, M.A., 1981. Wave-induced responses in a fluid-filled poro-elastic solid with a free surface-a boundary layer theory. Geophys. J. Int. 66, 597–631.
Okusa, S., 1985. Wave-induced stress in unsaturated submarine sediments. Géotechnique 35, 517–532.
Olsson, E., Kreiss, G., Zahedi, S., 2007. A conservative level set method for two phase flow II. J. Comput. Phys. 225, 785–807.
Rodi, W., 1993. Turbulence Models and Their Application in Hydraulics-state-of-the Art Review 3rd edition. Balkema, Rotterdam, the Netherlands.
Thomas, S.D., 1989. A finite element model for the analysis of wave induced stresses, displacements and pore pressures in an unsaturated seabed. I: Theory. Comput. Geotech. 8, 1–38.
Turcotte, B.R., Kulhawy, F.H., Liu, P.L., 1984. Laboratory evaluation of wave tank parameters for wave-sediment interactionSchool of Civil and Environmental Engineering. Cornell University, New York.
Ulker, M., Rahman, M., Jeng, D.S., 2009. Wave-induced response of seabed: various formulations and their applicability. Appl. Ocean Res. 31, 12–24.
Yamamoto, T., Koning, H., Sellmeijer, H., Hijum, E.V., 1978. On the response of a poro-elastic bed to water waves. J. Fluid Mech. 87, 193–206.
Ye, J.-H., Jeng, D.-S., 2011a. Effects of bottom shear stresses on the wave-induced dynamic response in a porous seabed: PORO-WSSI (shear) model. Acta Mech. Sin. 27, 898–910.

Ye, J.H., Jeng, D.S., 2011b. Response of porous seabed to nature loadings: waves and currents. J. Eng. Mech. 138, 601–613.
Zen, K., Yamazaki, H., 1990. Mechanism of wave-induced liquefaction and densification in seabed. Soils Found. 30, 90–104.
Zhang, X.L., Jeng, D.S., Luan, M.T., 2011. Dynamic response of a porous seabed around pipeline under three-dimensional wave loading. Soil Dyn. Earthq. Eng. 31, 785–791.
Zhang, Y., Jeng, D.S., Gao, F.P., Zhang, J.S., 2013. An analytical solution for response of a porous seabed to combined wave and current loading. Ocean Eng. 57, 240–247.
Zhao, H.-Y., Jeng, D.-S., Guo, Z., Zhang, J.S., 2014. Two-dimensional model for pore pressure accumulations in the vicinity of a buried pipeline. J. Offshore Mech. Arct. 136, 042001.
Zhao, H.-Y., Jeng, D.-S., 2016. Accumulated pore pressures around submarine pipeline buried in trench layer with partial backfills. J. Eng. Mech. 142, 04016042.
Zhao, H.-Y., Jeng, D.-S., Liao, C.C., 2016. Effects of cross-anisotropic soil behavior on the wave-induced residual liquefaction in the vicinity of pipeline buried in elasto-plastic seabed foundations. Soil Dyn. Earthq. Eng. 80, 40–55.
Zienkiewicz, O.C., Chang, C.T., Bettess, P., 1980. Drained, undrained, consolidating and dynamic behaviour assumptions in soils. Géotechnique 30, 385–395.